Fermi National Accelerator Laboratory

FERMILAB-Conf-00/078-E
CDF

Hard Diffraction at CDF

Andrei Solodsky

The Rockefeller University
1230 York Avenue, New York, New York 10021

Fermi National Accelerator Laboratory
P.O. Box 500, Batavia, Illinois 60510

April 2000

Presented at and to appear in the Published Proceedings of the *International Conference on Elastic and Diffractive Scattering*, Protvino, Russia, June 28-July 2, 1999

HARD DIFFRACTION AT CDF

ANDREI SOLODSKY
The Rockefeller University, 1230 York Avenue, New York, NY 10021, USA
E-mail: solodsky@physics.rockefeller.edu

We summarize published results on diffractive dijet and W production and review new results on diffractive beauty and J/ψ production using the rapidity gap method to tag diffraction. The diffractive structure function of the proton obtained from the analysis of dijet events with a leading antiproton is discussed and compared with expectations based on results obtained in deep inelastic scattering experiments at HERA. Also we report on recent results of dijet production in double pomeron exchange.

1 Introduction

To study diffractive production at CDF we used two different methods. One is by searching for *rapidity gaps*, which are pseudorapidity [1] regions devoid of particles, in the event topology. We applied this method to diffractive dijet [2], W [3] and heavy flavor [4] production measurements, described in sections 2 and 3. Another technique is the direct measurement of the diffractively scattered antiproton with a forward Roman pot spectrometer.

The CDF detector is described elsewhere [5]. Charged tracks in the region $|\eta| < 1.1$ are detected in the central tracking chamber (CTC) surrounded by the central and end-plug calorimeters. The microstrip silicon vertex detector (SVX) provides spatial measurement in the $r - \phi$ plane with a track impact parameter resolution of $\approx [13 + 40(\mathrm{GeV/c})/p_T]$ μm. The parts of the detector most relevant for the rapidity gap analyses are the forward calorimeters and the beam-beam counters (BBC). The fiducial region of the forward calorimeters covers the range $2.4 < |\eta| < 4.2$. The BBC consist of two arrays of eight vertical and eight horizontal scintillation counters which cover approximately the region $3.2 < |\eta| < 5.9$.

2 Diffractive Dijet and W Production

CDF searched for diffractive dijet production in a sample of dijet events with a single-vertex in which the two leading jets with transverse energy [1] $E_T >$ 20 GeV are both at $\eta < -1.8$ or $\eta > 1.8$. The single diffractive production was observed in these events by the requirement of a rapidity gap in both the forward calorimeter and the beam-beam counters (BBC) on one side of the detector.

Figure 1 shows the correlation of the BBC and forward calorimeter tower multiplicities in the η-region opposite the dijet system. The distinct excess in the (0,0) bin is associated with diffractive production. After subtracting the non-diffractive background and correcting for the losses caused by extra $\bar{p}p$ interactions in the same bunch crossing as a diffractive event, as well as for BBC and forward calorimeter live time acceptance and for the rapidity gap acceptance (0.70 ± 0.03), calculated using the POMPYT[6] Monte Carlo program with pomeron $\xi < 0.1$, the fraction of diffractively produced dijet events was found to be

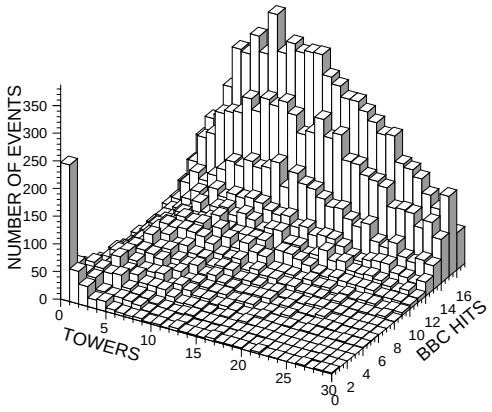

Figure 1. BBC hits versus forward calorimeter towers in region opposite a forward dijet.

$$R_{JJ} = [0.75 \pm 0.05(stat) \pm 0.09(syst)]\%.$$

In addition, CDF studied diffractive W production [3], which results predominantly from $q\bar{q}$ annihilation and probes the quark/antiquark content of the pomeron, using a sample of events with an isolated central e^+ or e^- ($|\eta| < 1.1$) of $E_T > 20$ GeV and missing transverse energy $\not\!\!E_T > 20$ GeV. The ratio of single diffractive to non-diffractive W production in this analysis was determined to be

$$R_W = [1.15 \pm 0.51(stat) \pm 0.20(syst)]\% \quad (\xi < 0.1).$$

Since diffractive dijet production is mostly sensitive to gluons in the pomeron, we can combine the dijet and W measurements and determine the gluon fraction in the pomeron[2], $f_g = 0.7 \pm 0.2$, which is consistent with the gluon fraction found by the ZEUS experiment [7].

3 Diffractive Heavy Flavor Production

We extended our studies of diffractive processes to diffractive heavy flavor production, charm and beauty, to probe directly the gluon content of the pomeron. Our diffractive beauty [4] production measurement is based on identifying a high transverse momentum electron with $E_T > 9.5$ GeV and $|\eta| < 1.1$, from the semi-leptonic b-quark decay, produced in single diffraction

dissociation, $p + \bar{p} \to p/\bar{p} + b(\to e + X') + X$. Each event is required to have a jet consisting of at least two tracks in addition to the electron candidate.

First, we extract a diffractive signal from the obtained event sample and then estimate the b-quark fraction separately in the diffractive and total event samples.

As in our previous analyses [2,3], the diffractive signal is extracted by counting BBC hits, N_{BBC}, and adjacent forward calorimeter towers, N_{CAL}, with $E > 1.5$ GeV. Figure 2(a) shows the correlation between N_{BBC} and N_{CAL} for both the positive and negative η sides of the detector, i.e. two entries per event. The (0,0) bin contains 100 events. We evaluate the non-diffractive content of the (0,0) bin from the distribution of events along the diagonal of Fig. 2(a), with $N_{BBC} = N_{CAL}$, shown in Fig. 2(b) by extrapolating a fit to the data of bins (2,2) to (9,9) to bin (0,0). This yields 24.4 ± 5.5 non-diffractive background events in the (0,0) bin.

Figures 2(c) and 2(d) show the electron E_T and η distribution, respectively, for the diffractive (points) and total (histogram) event samples. In Fig. 2(d), the sign of η of diffractive events with a gap at positive η was changed, so that the gap always appears at negative η. While the E_T spectra show no significant difference, the diffractive η distribution is shifted away from the gap relative to the symmetric distribution of the total event sample, in agreement with the single diffraction event topology.

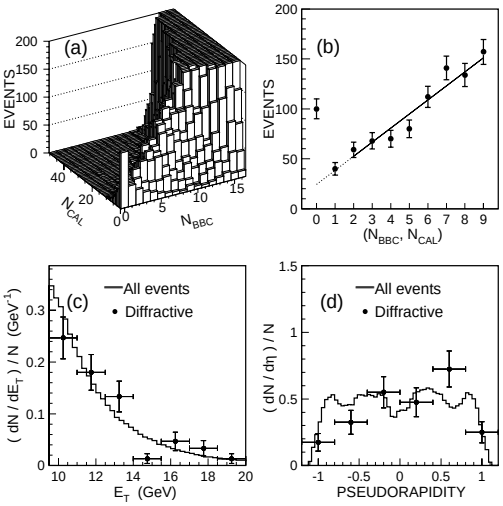

Figure 2. (a) Beam-beam counter multiplicity, N_{BBC}, versus forward calorimeter tower multiplicity, N_{CAL}; (b) multiplicity distribution along the diagonal with $N_{BBC} = N_{CAL}$ in the plot in (a); (c) electron p_T and (d) pseudorapidity for the diffractive (points) and total (histogram) event samples.

In addition to events from b-quark decays, the data contain events from charm decays and background. The background is mainly due to electrons from residual photon conversions and to hadrons faking electrons.

We use two methods to extract the fraction of beauty events in the data. In the first method, we fit the electron momentum component perpendicular to the jet axis, $p_T^{e/jet}$, which depends on the mass of the parent quark, with

the sum of four templates: photon conversions, fake electrons from hadrons, charm and beauty. This fit yields a beauty fraction of $(42.9 \pm 0.4)\%$ $[(38 \pm 14)\%]$ for the total [diffractive] event sample. The second method uses the impact parameter of the electron track, which is defined as the minimum distance between the primary vertex and the electron track in the $r-\phi$ plane and depends on both the mass and the lifetime of the parent quark. A fit to the impact parameter distribution using four templates, as above, yields $(47.7 \pm 0.4)\%$ $[(38 \pm 14)\%]$ for our two data samples.

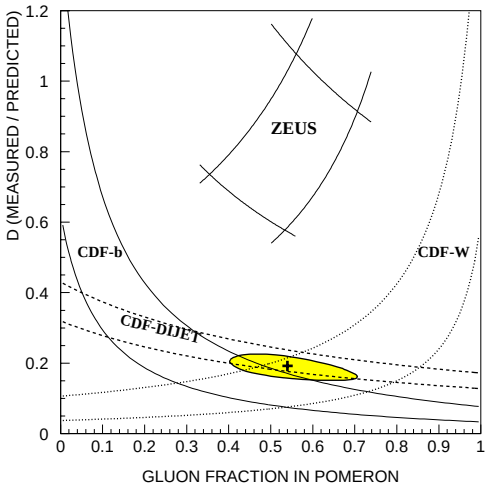

Figure 3. The ratio D of measured to predicted diffractive rates as a function of the gluon content of the pomeron.

The average of the results of both methods yields $73371 \pm 485(stat) \pm 7774(syst)$ $[44.4 \pm 10.2(stat) \pm 4.7(syst)]$ beauty events for the total [diffractive] event sample. The difference between the results of the two methods is assigned as systematic uncertainty. After subtracting the 24% non-diffractive background estimated from the fit in Fig. 2(b), there remain $33 \pm 10(stat) \pm 5(syst)$ diffractive beauty events. Correcting the diffractive event yield for single-vertex selection cut efficiency (0.26 ± 0.01), and for the detector live-time acceptance (0.77 ± 0.07) due to noise or beam associated background, we obtain $165 \pm 50(stat) \pm 29(syst)$ diffractive beauty events.

The diffractive to total b-quark production ratio obtained from the above numbers is $R_{bb}^{gap} = [0.23 \pm 0.07(stat) \pm 0.05(syst)]\%$. The rapidity gap acceptance for events generated using POMPYT Monte Carlo with a flat pomeron structure, which is favored by HERA measurements [7,8], and a gluon to quark ratio of 0.7 ± 0.2, as reported in ref. 2, is found to be 0.37 ± 0.02. Dividing $R_{\bar{b}b}^{gap}$ by this value yields a diffractive to total production ratio of

$$R_{\bar{b}b} = [0.62 \pm 0.19(stat) \pm 0.14(syst)]\% \quad (\xi < 0.1).$$

POMPYT with the standard pomeron flux and a flat (hard) pomeron structure consisting of purely gluons or quarks yields $R_{\bar{b}b}$ of 10.4%(11.6%) and 0.92%(1.02%), respectively. The ratio D of the measured $R_{\bar{b}b}$ fraction to that predicted by POMPYT depends on the gluon fraction f_g of the pomeron. This dependence is shown in Fig. 3, where D is plotted as a function of f_g

along with published results from ZEUS and CDF measurements [2,3]. For each measurement the two curves show the 1σ bounds. The black cross and shaded ellipse represent the best fit and 1σ contour of a least square two-parameter fit to the three CDF results. The fit yielded $D_{CDF} = 0.19 \pm 0.04$ and $f_g^{CDF} = 0.54^{+0.16}_{-0.14}$, in agreement with the results we obtained from the W and dijet rates, namely $D = 0.18 \pm 0.04$ and $f_g = 0.7 \pm 0.2$ [2]. The value of D_{CDF} is significantly smaller than the ZEUS result. The discrepancy between the HERA and Tevatron D-values represents a breakdown of factorization. The observed discrepancy is in general agreement with predictions based on the renormalized pomeron flux model [9].

We also searched for diffractive J/ψ production in a sample of central ($|\eta| < 1.1$) dimuons. For J/ψ reconstruction we required a pair of opposite charge muons with $p_T > 2$ GeV/c and invariant mass close to the J/ψ mass. The technique we used to extract the diffractive signal is identical to that used in our previous studies. Preliminary results of this analysis, before correcting for the gap acceptance A, give a ratio of diffractive to non-diffractive J/ψ production of

$$R_{J/\psi} \times A = [0.36 \pm 0.07]\%.$$

In spite of the fact that all diffractive processes studied at CDF are differently sensitive to the quark and gluon content of the pomeron, the obtained ratios of diffractive to non-diffractive production are all of the same order of magnitude, $\sim 1\%$. This indicates that the structure of the pomeron probed in single diffraction events is not very different from the structure of the proton.

4 Study of Diffractive Structure Function

In the beginning of 1996 a forward Roman pot spectrometer (RPS) was added to CDF to detect diffractive antiprotons, which carry away a fraction x_F, measured by RPS, of their original momentum. The fraction of the $\bar{p}$ momentum taken by the pomeron is $\xi = 1 - x_F$; the momentum fraction of the parton in the pomeron, β, is given by $\beta = x/\xi$, where x is the fraction of the momentum of the $\bar{p}$ carried by the struck parton.

From an inclusive sample of single diffraction (SD) events, collected by triggering on a recoil $\bar{p}$ detected in the RPS, we selected events containing at least two jets with transverse energy $E_T^{jet} > 7$ GeV. For the non-diffractive (ND) dijet sample we used data collected with a minimum bias (MB) trigger requiring a coincidence of the BBCs in the p and $\bar{p}$ directions. From the E_T and η of the jets (including a third jet if $E_T^{jet3} > 5$ GeV) we determine the

fraction x of the momentum of the antiproton carried by the struck parton,

$$x = \frac{1}{\sqrt{s}} \sum_{i=1}^{n} E_T^i e^{-\eta^i}.$$

Since the ratio $R(x)$ of the SD to ND dijet cross sections is equal to the ratio of the antiproton SD to ND structure functions, the diffractive structure function may be obtained by multiplying the known ND structure by $R(x)$. The SD dijet sample is normalized by scaling its event rate to that of the inclusive diffractive sample and using for the latter the measured [10] *soft* SD cross section. The absolute normalization of the ND dijet sample is obtained from the measured 51.2 ± 1.7 mb cross section of the BBC trigger.

The data were collected during runs of typical luminosities $\sim 3 \times 10^{29}\ cm^{-2}sec^{-1}$. We selected events with only one reconstructed vertex within $|z_{vtx}| < 60$ cm, and applied quality cuts to ensure that a reconstructed Roman pot track, assumed to originate at the primary vertex, is a diffracted $\bar{p}$. In the resulting *inclusive* sample of 1.6 million SD and 300K MB events, we observed 30,410 SD and 32,629 ND events containing at least two jets of corrected $E_T^{jet} > 7$ GeV. The E_T of a jet was defined as the sum of the calorimeter E_T within an $\eta - \phi$ cone [11] of radius 0.7.

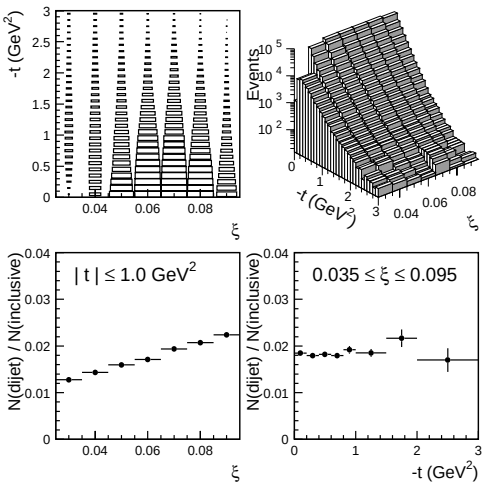

Figure 4. Distributions versus ξ and t: (a) Roman pot acceptance; (b) inclusive diffractive event sample; (c) rato of dijet to inclusive diffractive events versus ξ and (d) versus t.

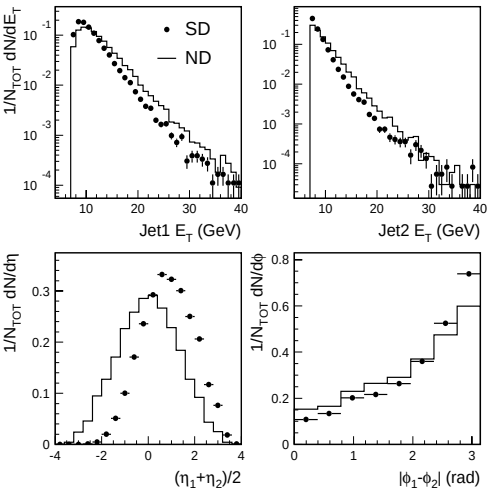

Figure 5. Comparison of diffractive to non-diffractive dijet events: (a) Leading jet E_T; (b) next to leading jet E_T; (c) mean η of dijet system; (d) azimuthal angle difference between the two leading jets.

In the jet energy correction the underlying event energy with an average

E_T of 0.54 (1.16) GeV was subtracted from each jet in SD (ND) events. These values were determined experimentally from the $\sum E_T$ of calorimeter tower energy measured within a randomly chosen η-ϕ cone of radius 0.7 in events of the inclusive data samples.

Figures 4(a) and 4(b) show, respectively, the RPS acceptance and a lego plot of the inclusive diffractive event sample as a function of ξ and t. The acceptance is large for ξ in the range of 0.04 to 0.1 and for $|t| < 1$ GeV^2. The fraction of dijet events in the inclusive sample is shown as a function of ξ in Fig. 4(c) and versus t in Fig. 4(d). We observe that while the fraction of dijet events increases linearly as a function of ξ, there is no significant t dependence in the region $0 < |t| < 3$ GeV^2, in agreement with the UA8 result [12].

Figure 5 shows distributions of E_T^{jet1}, E_T^{jet2}, $\bar{\eta} = (\eta^{jet1} + \eta^{jet2})/2$ and $\Delta\phi = \phi^{jet1} - \phi^{jet2}$ for the diffractive (points) and ND (histograms) event samples. The E_T^{jet1} and E_T^{jet2} distributions fall faster in the SD than in the ND events. This is due to the difference in SD and ND structure functions (see below). The diffractive dijets are boosted away from the leading antiproton in η (the $\bar{p}$ is at negative η). The diffractive $\Delta\phi$ distribution is narrower, jets being more back-to-back, than the ND.

The ratio $\tilde{R}(x)$ of the number of SD dijet events, corrected for Roman pot acceptance, to the number of ND dijets is shown in Fig. 6 for six bins in ξ of width 0.01 ranging from 0.035 to 0.095. The two data samples are normalized to correspond to the same luminosity. The tilde over the R indicates integration over variables (t, ξ, E_T^{jet}) for diffractive and E_T^{jet} for ND events. The results are shown in Fig. 6 for $|t| < 1$ GeV^2 and $E_T(jet1, jet2) > 7$ GeV. The data points are well fit by lines of the form $\tilde{R}(x) = R_0(x/0.0065)^{-r}$ in the region $10^{-3} < x < 0.5\xi_{min}$ for each ξ-bin. The lower x limit is imposed to minimize detector end-effects. The shape of the $\tilde{R}(x)$ distribution shows no significant ξ dependence. A fit to all the data in the region $0.035 < \xi < 0.095$ yields

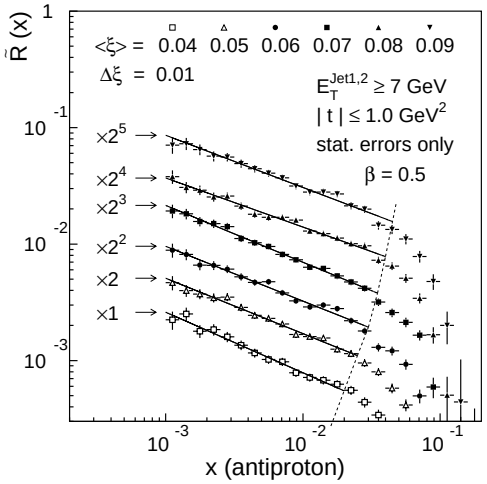

Figure 6. Ratio of diffractive to non-diffractive dijet event rates as a function of x (momentum fraction of parton in $\bar{p}$). The solid lines are fits to the form $\tilde{R}(x) = R_0(x/0.0065)^{-r}$ for $\beta < 0.5$, where $\beta = x/\langle\xi\rangle$.

$R_0 = (6.2 \pm 0.1) \times 10^{-3}$ and $r = 0.45 \pm 0.02$ with χ^2/d.o.f. $= 0.72$.

The diffractive and ND structure functions can be written in terms of gluon and quark densities as $F_{jj}(x) = x[g(x) + \frac{4}{9}q(x)]$, where $\frac{4}{9}$ is a color factor. As mentioned above, $R(x)$ represents the ratio of the diffractive to ND structure functions of the antiproton. Thus, we can determine the diffractive structure function of the antiproton by the formula

$$\tilde{F}_{jj}^{D}(\beta) = \tilde{R}(x = \beta\xi) \times \tilde{F}_{jj}^{ND}(\beta),$$

where we change variables to $\beta = x/\xi$. We have evaluated $\tilde{F}_{jj}^{D}(\beta)$ for $|t| < 1$ GeV^2, $0.035 < \xi < 0.095$ and $E_T(jet1, jet2) > 7$ GeV using the GRV92LO parton densities [13] in $\tilde{F}_{jj}^{ND}(\beta)$. The obtained $\tilde{F}_{jj}^{D}(\beta)$ is shown in Fig. 7, where the solid line is a fit to the data of the form $\tilde{F}_{jj}^{D}(\beta) = B(\beta/0.1)^{-n}$ in the range $(10^{-3}/\xi) < \beta < 0.5$. The fit yields $B = 1.15 \pm 0.01$ and $n = 1.09 \pm 0.01$ with χ^2/d.o.f. $= 2.2$. For our average ξ of 0.065 the value of $\beta = 0.1$, for which $\tilde{F}_{jj}^{D} = B$, corresponds to $x = 0.0065$, for which $\tilde{R} = R_0$. The lower and upper boundaries of the filled band surrounding the data points represent the β-distributions obtained by using only the two leading jets or up to four jets of $E_T > 5$ GeV, respectively, in the evaluation of x. The dashed (dotted) curve is obtained from fit 2 (fit 3) of the H1 diffractive structure function [8] evaluated at $Q^2 = 75$ GeV^2, which approximately corresponds to the average value of $(E_T^{jet})^2$ of our data. The measured and expected structure functions disagree both in normalization and shape. The discrepancy in normalization, defined as the integral over β of data over expectation, is $D = 0.06$ (0.05) for fit 2 (fit 3). The disagreement between our measured diffractive structure function and the expectation from diffractive DIS represents a breakdown of factorization similar to that observed [2] in comparing diffractive W-boson and dijet production rates with expectations based on ZEUS results [7] obtained from diffractive DIS and dijet photoproduction at HERA.

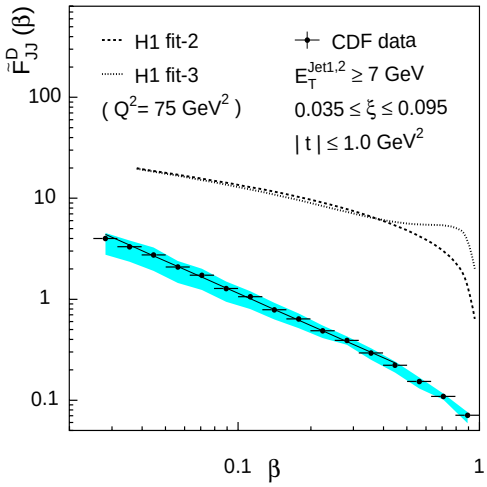

Figure 7. Data β distribution (points) compared with expectations from the parton densities of the proton extracted from diffractive deep inelastic scattering by the H1 Collaboration. The solid line is a fit to the data of the form β^{-n} in the indicated region. The dashed (dotted) lines are expectations from the H1 fit 2 (fit 3).

5 Dijets in Double Pomeron Exchange

Using the data sample obtained by triggering on an outgoing $\bar{p}$ with the RPS, we searched for dijet production by Double Pomeron Exchange (DPE). In these events the jets are produced in the central region, separated from the diffractive p and $\bar{p}$ by large rapidity gaps. From an inclusive sample of single diffractive events with detected diffractive $\bar{p}$, we selected events containing at least two jets with $E_T^{jet} > 7$ GeV and than searched for a DPE signal by looking for a rapidity gap on the p side, using the BBC array and forward calorimeters. Figure 8(a) shows a 2-dimensional plot of the BBC multiplicity, N_{BBC}, and forward calorimeter tower multiplicity, N_{CAL}, on the proton side. The excess in the (0,0) bin is attributed to DPE production of jets. We used the diagonal bins ($N_{BBC} = N_{CAL}$) of Fig. 8(a) to evaluate the contribution from low multiplicity SD events in the (0,0) bin. The diagonal multiplicity distribution is shown in Fig. 8(b).

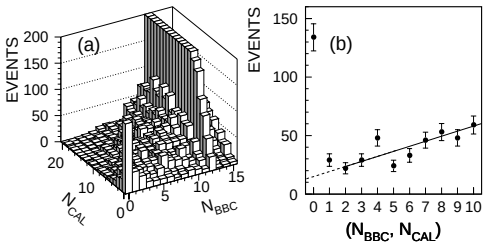

Figure 8. (a) BBC hit multiplicity, N_{BBC}, versus forward calorimeter tower multiplicity, N_{CAL}; (b) multiplicity distribution along the diagonal with $N_{BBC} = N_{CAL}$ in (a).

The measured production ratios of DPE to SD, SD to ND and DPE to ND for dijet events in the kinematic range $0.04 < \xi_{\bar{p}} < 0.095$, $|t| < 1$ GeV^2 for SD and DPE, and estimated $0.05 < \xi_p < 0.035$ for DPE, are presented in the table below:

R_{SD}^{DPE}	$0.40 \pm 0.04 \pm 0.08\,\%$
R_{ND}^{SD}	$0.31 \pm 0.004 \pm 0.03\,\%$
R_{ND}^{DPE}	$[1.3 \pm 0.1 \pm 0.4] \times 10^{-5}$

Figure 9 shows the distributions of E_T^{jet1}, E_T^{jet2}, $\eta^* \equiv (\eta^{jet1} + \eta^{jet2})/2$ and $\Phi \equiv \Phi^{jet1} - \Phi^{jet2}$ for the DPE (points), SD (solid histograms) and ND (dashed histograms) dijet events. The E_T^{jet} spectrum of DPE dijets is similar

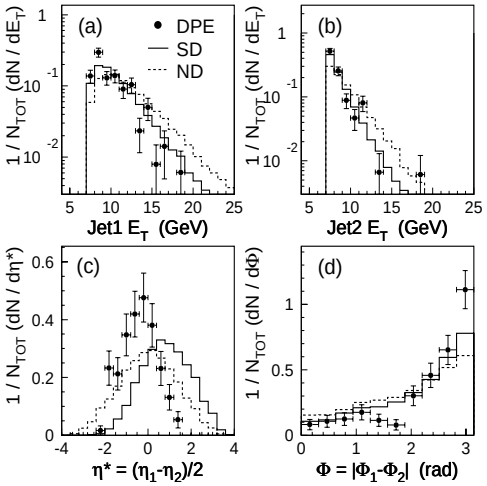

Figure 9. Dijet kinematics of the DPE events (points) compared with single diffractive (non-diffractive) dijet events shown as the solid (dashed) line: (a) Leading jet E_T; (b) next to leading jet E_T; (c) mean η of dijet system; (d) azimuthal angle difference between the two leading jets.

to that of SD jets, and slightly steeper than that of ND dijets. The η^* distribution shows that DPE dijets are boosted toward the negative η ($\bar{p}$ direction), in contrast to the SD dijets, which are boosted toward the p side, and the ND dijets, which are produced symmetrically. This behavior can be explained by the difference between ξ_p and $\xi_{\bar{p}}$ ($\xi_p < \xi_{\bar{p}}$). The DPE dijets are produced more back-to-back than the SD and ND dijets.

Acknowledgments

We thank the Fermilab staff and the technical staffs of the participating institutions for their vital contributions. This work was supported by the U.S. Department of Energy and National Science Foundation; the Italian Istituto Nazionale di Fisica Nucleare; the Ministry of Education,Science and Culture of Japan; the Natural Sciences and Engineering Research Council of Canada; the National Science Council of the Republic of China; and the A. P. Sloan Foundation; the Max Kade Foundation; and the German Landes-Ministry.

References

1. We use rapidity and pseudorapidity, η, interchangeably; $\eta \equiv -\ln(\tan\frac{\theta}{2})$, where θ is the polar angle of a particle with respect to the proton beam direction. The azimuthal angle is denoted by ϕ, and the transverse energy of a jet, E_T^{jet}, is defined as $E^{jet}\sin\theta$.
2. F. Abe *et al.*, *Phys. Rev. Lett.* **79**, 2636 (1997).
3. F. Abe *et al.*, *Phys. Rev. Lett.* **78**, 2698 (1997).
4. T. Affolder *et al.*, submitted to Phys. Rev. Lett.
5. F. Abe *et al.*, *Nucl. Instrum. Methods* A **271**, 387 (1988).
6. P. Bruni, A. Edin and G. Ingelman, Report No. DESY-95, DRAFT, ISSN 0418-9833; http://www3.tsl.uu.se/thep/pompyt/
7. M. Derrick *et al.*, *Z. Phys.* C **68**, 569 (1995); *Phys. Lett.* B **356**, 129 (1995); *Eur. Phys. J.* A **6**, 43 (1999).
8. T. Ahmed *et al.*, *Phys. Lett.* B **348**, 681 (1995); C. Adloff *et al.*, *Z. Phys.* C **76**, 613 (1997).
9. K. Goulianos, *Phys. Lett.* B **358**, 379 (1995); B **363**, 268 (1995).
10. F. Abe *et al.*, *Phys. Rev.* D **50**, 5518 (1994); D **50**, 5535 (1994); D **50**, 5550 (1994).
11. F. Abe *et al.*, *Phys. Lett.* B **45**, 1448 (1992).
12. A. Brandt *et al.*, *Phys. Lett.* B **297**, 417 (1992); B **421**, 395 (1998).
13. M. Glück, E. Reya and A. Vogt, *Z. Phys.* C **53**, 127 (1992).